RSC Advances

PAPER

View Article Online
View Journal | View Issue

Cite this: *RSC Adv.*, 2017, **7**, 33364

Two novel Co(II) and Ni(II) complexes of tebuconazole with enhanced antifungal activities†

Jie Li,[a] Yao Zhang,[a] Mingyan Yang[b] and Haixia Ma *[a]

Received 29th March 2017
Accepted 24th June 2017

DOI: 10.1039/c7ra03629a

rsc.li/rsc-advances

Two transition metal complexes, $[CoL_4Cl_2]\cdot 4MeOH$ **1** and $[NiL_4Cl_2]\cdot 4MeOH$ **2** (L = (RS)-1-(4-chloro-phenyl)-4,4-dimethyl-3-(1,2,4-triazole-1-ylmethyl)pentane-3-ol), tebuconazole were synthesized and their structures were determined using single crystal X-ray diffraction (XRD). Crystal structural analysis shows that complexes **1** and **2** have similar structures, both with the metal cation lying on a crystallographic inversion center and coordinated with four triazole groups and two chloride anions. The antifungal activities of L and its complexes against four selected plant pathogenic fungi were evaluated. The results show that both complexes have stronger bioactivities than the ligand L and that complex **2** has slightly higher bioactivities than complex **1**. To elucidate the mechanisms behind the increased antifungal activities of the title complexes in comparison with L, cumulative release studies in static water and theoretical investigations of the complexes were carried out. The results indicate that there are three factors contributing to the enhanced bioactivities: attractive controlled release properties, synergic interaction between metal cations and L, and improved penetration into the lipid membranes.

1 Introduction

Although complexes containing transition metals and multidentate ligands have been extensively investigated over the past decades due to their unique structures[1–3] and potential applications in different fields,[4–8] studies on the complexation of commercial 1,2,4-triazole fungicides with transition metals are still rare. Evans reported the formation and structures of $CuAc_2$ and $ZnAc_2$ complexes with tebuconazole and propiconazole.[9] Yang reported the synthesis, controlled release properties and antifungal activities of a series of metal complexes with *cis* and *trans* propiconazole.[10] Fujii prepared difenoconazole copper complexes and used them as wood preservatives.[11] Our group reported the structures and antifungal activities of two Cu(II) complexes with triadimefon[12] and four Cu(II) complexes with tebuconazole.[13] In the literature, it has been shown that the pharmacological and toxicological properties of many drugs are modified when they form metallic complexes.[10–15] Complexation of pesticides with metals has potential advantages including the enhancement of persistence, longer shelf life, reduction of mammalian toxicity and conversion of pesticides from non-systemic to systemic.[16–18] Moreover, the pesticides coordinated with transition metals could be utilized for controlled release formulations with the capacity of alleviating the toxicity and decreasing the pesticide residue.[10,19]

Tebuconazole ($C_{16}H_{22}ClN_3O$, CASRN: 107534-96-3), chemically named (RS)-1-(4-chloro-phenyl)-4,4-dimethyl-3-(1,2,4-triazole-1-ylmethyl)pentane-3-ol, is an important 1,2,4-triazole fungicide with broad bactericidal spectrum, high antibacterial efficiency and low toxicity, which has been widely used to control mildews and rusts of cereal grains, fruits, vegetables and ornamentals by inhibiting the synthesis of ergosterol to prevent fungal mycelium development.[20–22] However, the intensive use of tebuconazole and their single active site have led to substantial environmental contamination and a rapid selection of resistance strains.[23–25] Given the limitations of tebuconazole and with the aim of possibly improving its properties and potential applications, a series of metal complexes with tebuconazole have been studied in our lab.

In an earlier study, we reported four Cu(II) complexes of tebuconazole[13] and found that the obtained copper complexes exhibited potent antifungal activity toward the selected fungi *Gibberella nicotiancola*, *Botryosphaeria berengriana*, *Botryosphaeria ribis*, *Alternaria solani*. To continue our work on the complexes with tebuconazole and study the impact of different metal cations (Co^{2+} and Ni^{2+}) on the crystal structures and the bioactivities, in this work, we have conducted experimental and theoretical investigations on the molecular and electronic structures of $[CoL_4Cl_2]\cdot 4MeOH$ **1** and $[NiL_4Cl_2]\cdot 4MeOH$ **2**. Meanwhile, the antifungal activities of these two complexes against four selected plant pathogenic fungi and the possible reasons for the increased bioactivities after complexation are also discussed.

[a]*School of Chemical Engineering, Northwest University, Xi'an, Shaanxi 710069, China. E-mail: mahx@nwu.edu.cn; Fax: +86-029-88307755; Tel: +86-029-88307755*

[b]*Department of Environmental Science and Engineering, Chang'an University, Xi'an, Shaanxi 710054, China*

† CCDC 934445 **1** and 934446 **2**. For crystallographic data in CIF or other electronic format see DOI: 10.1039/c7ra03629a

2 Results and discussion

2.1 Synthesis and IR spectroscopy

As shown in Scheme 1, reactions of tebuconazole with the inorganic metal salts $CoCl_2 \cdot 6H_2O$ and $NiCl_2 \cdot 6H_2O$ under the same reaction conditions led to similar mononuclear 1,2,4-triazole complexes with four ligands, two chloride anions and four free methanol molecules, namely, $[CoL_4Cl_2] \cdot 4MeOH$ **1** and $[NiL_4Cl_2] \cdot 4MeOH$ **2**.

The IR spectra of the complexes **1** and **2** show that both the complexes display characteristic bands of alcoholic hydroxyl groups and the alcoholic hydroxyl ν(O–H) stretching vibrations in the IR spectrums are present at 3288 cm^{-1} and 3291 cm^{-1}, respectively. The strong absorption bands at 1491 cm^{-1} and 1492 cm^{-1} in the IR spectra of **1** and **2**, respectively attribute to the ν(C=C) stretching vibration. The bands observed in the 3134–2876 cm^{-1} region are assigned to the C–H stretching vibrations.

2.2 Description of structures

2.2.1 Crystal structure of $[CoL_4Cl_2] \cdot 4MeOH$ 1. The structural plots of complex **1** are depicted in Fig. 1. As shown in Fig. 1a, **1** consists of one cobalt cation, four ligands, two chloride anions and four uncoordinated methanol molecules. Co cation lies on a crystallographic inversion center. Co atom and four coordinated N atoms from four triazole rings occupy the equatorial plane. The least-squares plane equation of the equatorial plane is $8.109x + 4.515y - 0.831z = 3.6393$ with the mean deviation from the plane 0 Å, which indicates that these five atoms form a perfect plane. And Co, Cl3 and $Cl3^i$ atoms occupy the axial position. The Co–Cl bond length is 2.5508 Å, much longer than the Co–N bond lengths (2.141 and 2.153 Å), thus forming an elongated octahedron around the Co atom. The dihedral angles of benzene ring planes and their attached triazole planes are respectively 87.1° and 103.2°. The triazole ring planes are coplanar with their symmetric planes, and approximately perpendicular to their adjacent triazole ring planes (dihedral angle 104.6°). The oxidation state of cobalt in complex **1** was verified to be +2 by three ways. First, according to the I.D. Brown approach,[26] the bond valence sums (BVS) calculations for Co bonds gave the values of 2.05, indicating the oxidation state of cobalt is +2. Second, the bond lengths of Co–N (2.153(4) Å and 2.141(5) Å) and Co–Cl (2.5508(16) Å) are all in good agreement with the reported coordination bond lengths of Co–N (2.026–2.287 Å) and Co–Cl (2.3641–2.5132 Å),[27–30] suggesting that the cobalt in complex **1** binds to N and Cl atoms *via* coordination bonds other than covalent bonds, which can further indicate that the oxidation state of cobalt is +2. Third, from the point of charge balance, the ligand tebuconazole keeps neutral since the bond lengths of the ligand have very small variation after complexation (the largest bond length deviation

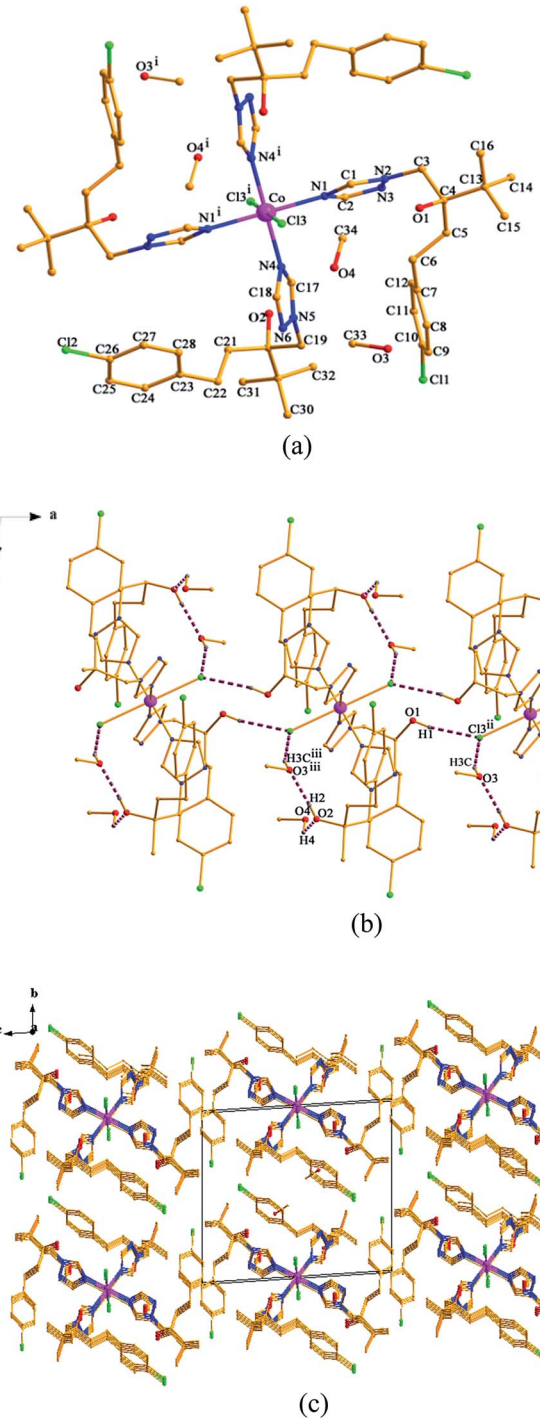

Fig. 1 Crystal structures of complex **1** (a) coordination mode (symmetry code: (i) $1 - x, -y, 1 - z$), hydrogen atoms are omitted for clarity. (b) 1D chain formed *via* hydrogen bonds along the *b*-axis. (symmetry code: (ii) $-x, -y, 1 - z$; (iii) $1 + x, y, z$). (c) Crystal packing along the *a*-axis.

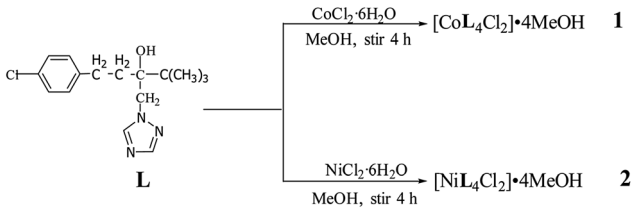

Scheme 1 Formation of the complexes with tebuconazole.

is 0.014 Å taking place in N2–N3). And Cl atom has the only reduction state of −1. To keep charge balancing, the oxidation state of cobalt should be +2.

As shown in Fig. 1b, there is one kind of intramolecular hydrogen bond O4–H4···O2 in the crystal structure of complex **1**, which is generated by the O4 atom of the free methanol molecule as hydrogen bond donor to O2 of the ligand. And there are three kinds of intermolecular hydrogen bonds: O1 and O3 atoms act as hydrogen bond donors to Cl3 atom from the adjacent molecule, generating O1–H1···Cl3^{ii} and O3–H3C···Cl3^{ii} (symmetry code: ^{ii} $-x, -y, 1-z$). Meanwhile, O2 atom also as hydrogen bond donor takes part in the hydrogen bonds of O2–H2···O3^{iii} (symmetry code: ^{iii} $1+x, y, z$). The intermolecular hydrogen bonds contribute to the formation of a one-dimensional chain along the *b*-axis in the crystal structure of complex **1**. Furthermore, the 1D chains are connected by van der Waals forces to give rise to the 3D framework along the *a*-axis, as shown in Fig. 1c.

2.2.2 Crystal structure of $[NiL_4Cl_2]\cdot 4MeOH$ 2. The structure of complex **2** is similar to that of **1**. As illustrated in Fig. 2a, each Ni(II) binds to four nitrogen atoms from four ligands and two chloride atoms leading to a distorted octahedral geometry. The bond lengths of Ni–N (2.080 Å, 2.094 Å) and Ni–Cl (2.4979 Å) are slightly shorter than the Co–N and Co–Cl bond lengths of complex **1**, which is due to the slightly smaller atomic radius of Ni (1.246 Å) than that of Co (1.253 Å).[31] In complex **2** the dihedral angles of benzene ring planes and their attached triazole planes are 88.4° and 104.2° respectively. The triazole ring planes are coplanar with their symmetric planes and approximately perpendicular to their adjacent triazole ring planes (dihedral angle 105.2°). All the related dihedral angles are close to those of complex **1**. The oxidation state of nickel in complex **2** was also determined to be +2 and the BVS calculations for Ni bonds in complex **2** gave the value of 2.17.

Unlike complex **1**, complex **2** only has intermolecular hydrogen bonds: O2 and O3 atoms act as hydrogen bond donors to Cl3 atom from the adjacent molecule, generating O2–H2···Cl3^{ii} and O3–H3···Cl3^{ii} (symmetry code: ^{ii} $1-x, 1-y, 1-z$). O1 atom as hydrogen bond donor takes part in hydrogen bond of O1–H1···O3^{iii} (symmetry code: ^{iii} $-1+x, y, z$). Meanwhile, O1 atom acts as hydrogen bond acceptor to O4 atom from the other adjacent molecule, generating O4–H4···O1^{iv} (symmetry code: ^{iv} $1+x, y, z$). Each structural unit of $[NiL_4Cl_2]\cdot 4MeOH$ is bound to two adjacent structural units by the intermolecular hydrogen bonds resulting in the formation of a one-dimensional chain along the *b*-axis (Fig. 2b). The 1D chains are also connected by van der Waals forces to form the 3D framework along the *a*-axis, as shown in Fig. 2c.

Structure refinement details of both the complexes are summarized in Table 1. Selected bond lengths and angles are listed in Table 2, and hydrogen bonds are shown in Table 3.

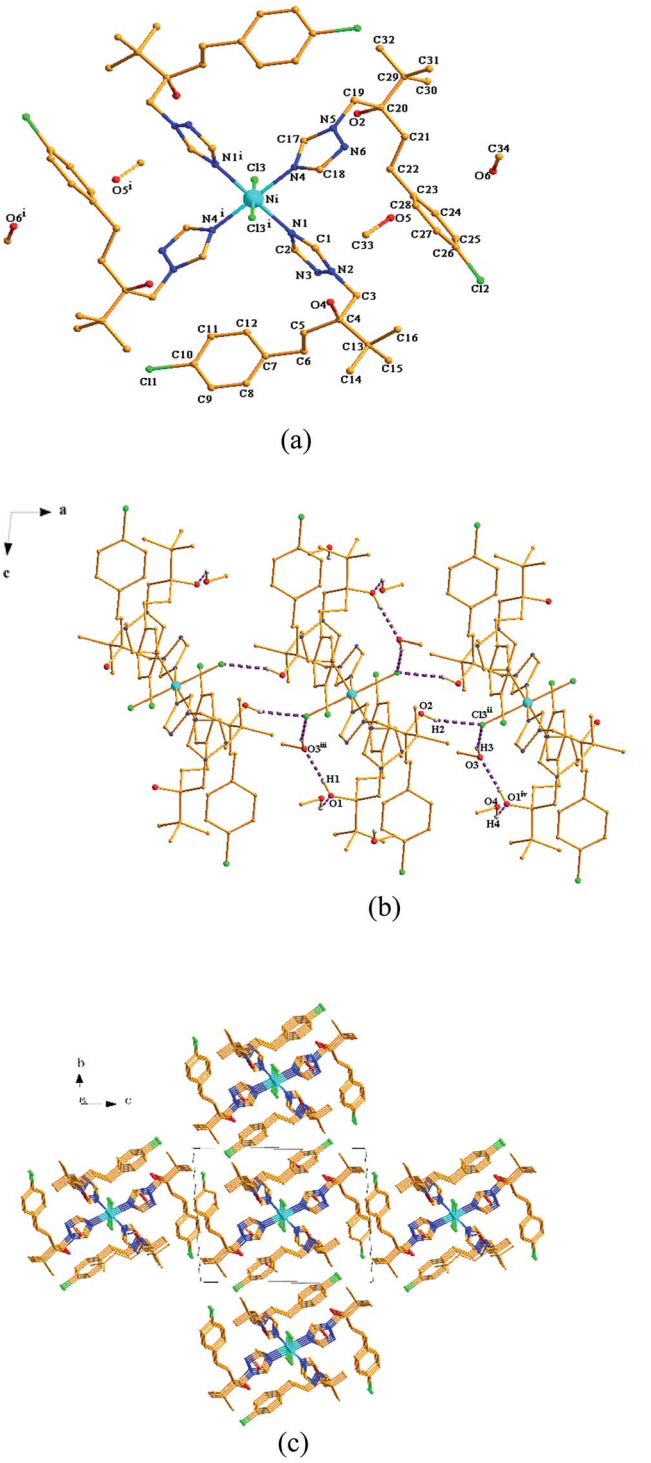

Fig. 2 Crystal structures of complex **2** (a) coordination mode (symmetry code: (i) $-x, 1-y, 1-z$), hydrogen atoms are omitted for clarity. (b) 1D chain formed *via* hydrogen bonds along the *b*-axis. (Symmetry code: (ii) $1-x, 1-y, 1-z$; (iii) $-1+x, y, z$; (iv) $1+x, y, z$). (c) Crystal packing along the *a*-axis.

2.3 Biological activities

2.3.1 Antifungal activities. As shown in Fig. 3, the inhibition rate increases with the growth of the concentration of ligand **L** and the complexes, and the inhibition rate at the same concentration is ranked as complex **2** > complex **1** > **L**. It can be seen from Table 4 that the synthesized metal complexes show higher antifungal activities than the ligand **L** against the four selected fungi, stronger antifungal activities than the reported

Table 1 Crystallographic data for **1** and **2**

Parameter	**1**	**2**
Empirical formula	$C_{68}H_{104}Cl_6CoN_{12}O_8$	$C_{68}H_{104}Cl_6NiN_{12}O_8$
Formula weight	1489.26	1489.04
Crystal size (mm)	0.31 × 0.27 × 0.24	0.32 × 0.25 × 0.21
Crystal system	Triclinic	Triclinic
Space group	*P*1	*P*1
a/(Å)	9.427(3)	9.350(3)
b/(Å)	14.221(5)	14.154(4)
c/(Å)	15.414(5)	15.270(4)
α/(°)	92.275(6)	92.110(6)
β/(°)	95.615(6)	95.644(6)
γ/(°)	101.926(6)	101.787(5)
V/(Å^3)	2008.3(12)	1965.3(10)
Z	1	1
D_c (g cm^{-3})	1.231	1.258
μ	0.469	0.508
F(000)	789	790
Reflns. collected	9940	9918
Unique/observed	7009/3305	6914/2733
$R_1(I \geq 2\sigma(I))$	0.0753	0.0830
wR_2 $(I \geq 2\sigma(I))$	0.1934	0.1820
Goodness-of-fit on F^2	0.957	0.933

Table 2 Selected bond lengths (Å) and angles (°) for complex **1** and **2**[a]

1		**2**	
Co–N1	2.153(4)	Ni–N1	2.080(6)
Co–N1^i	2.153(4)	Ni–N1^i	2.080(6)
Co–N4	2.141(5)	Ni–N4	2.094(5)
Co–N4^i	2.141(5)	Ni–N4^i	2.094(5)
Co–Cl3	2.5508(16)	Ni–Cl3	2.4979(18)
Co–Cl3^i	2.5508(16)	Ni–Cl3^i	2.4979(18)
N1–Co–N1^i	180.000(1)	N1–Ni–N1^i	180.000(1)
N4–Co–N4^i	180.000(1)	N4–Ni–N4^i	180.0(3)
Cl3–Co–Cl3^i	180.0	Cl3–Ni–Cl3^i	180.0
N1–Co–N4	90.38(17)	N1–Ni–N4	90.5(2)
N1–Co–Cl3	89.85(13)	N1–Ni–Cl3	89.32(16)

[a] Symmetry codes: complex **1** (i) $1-x, -y, 1-z$. Complex **2** (i) $-x, 1-y, 1-z$.

Table 3 Hydrogen bonds for complex **1** and **2**[a]

D–H···A	D–H	H···A	D···A	∠D–H···A
Complex 1				
O4–H4···O2	0.820	2.407	2.848	114.67
O2–H2···O3^{ii}	0.820	1.933	2.735	165.71
O1–H1···Cl3^{iii}	0.820	2.496	3.290	163.45
O3–H3C···Cl^{iii}	0.820	2.328	3.115	161.21
Complex 2				
O2–H2···Cl3^{ii}	0.820	2.477	3.266	161.76
O3–H3···Cl3^{ii}	0.820	2.283	3.086	166.07
O1–H1···O3^{iii}	0.820	1.915	2.725	169.16
O4–H4···O1^{iv}	0.820	2.279	2.837	125.67

[a] Symmetry code: complex **1** (ii) $-x, -y, 1-z$; (iii) $1+x, y, z$; complex **2** (ii) $1-x, 1-y, 1-z$; (iii) $-1+x, y, z$; (iv) $1+x, y, z$.

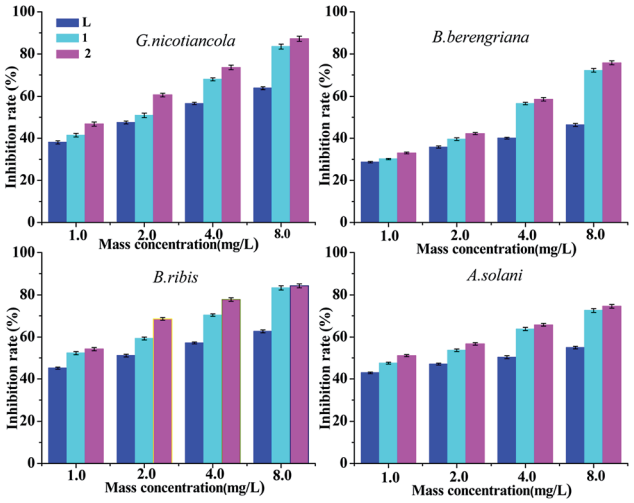

Fig. 3 Inhibition rate of the ligand **L** and the complexes. Values are given as mean ± SD.

Table 4 EC_{50} values of **L** and its complexes against plant pathogens (mg L^{-1})

Compound	*G. nicotiancola*	*B. berengriana*	*B. ribis*	*A. solani*
1	1.65	2.87	1.01	1.33
2	1.22	2.60	0.72	1.02
L	2.50	11.9	1.75	3.54
$CoCl_2 \cdot 6H_2O$	45.9	39.9	34.5	73.4
$NiCl_2 \cdot 6H_2O$	41.5	39.5	31.8	76.3

Cu complexes based on **L** against *G. nicotiancola* and *B. berengriana*,[13] and much stronger than the reported Cu complexes based on triadimefon against *G. nicotiancola* and *A. solani*.[12] From Table 4, we can also observe that the antifungal toxicities of complex **1** are 1.52–4.15 times greater than those of **L**, while the toxicities of complex **2** were 2.05–4.58 times higher than those of **L**. Overall, complex **2** is slightly more active than complex **1** in terms of the antifungal toxicities (complex **2** is 1.10–1.40 times better than complex **1**). However, for *B. berengriana*, complex **2** has almost equal antifungal activity to complex **1**.

2.3.2 Synergistic interaction between the metal cations and tebuconazole. The two complexes can be regarded as molecular-level mixtures of tebuconazole and metal cations, and Fig. 4 gives information of the interactions between the two metal cations and tebuconazole. Fig. 4 shows that all the values of SR are more than 1.5 (the minimum SR is 1.87), which indicates that the interaction levels were synergistic against the four selected fungi.[32] The result should be one reason for the enhanced bioactivities after complexation.

It is noteworthy that the interaction levels of complex **2** were higher than those of complex **1** for the same tested fungus. It indicates that the synergy levels for the molecular-level mixture of Ni^{2+} and tebuconazole were better than those for the molecular-level mixture of Co^{2+} and tebuconazole. This also

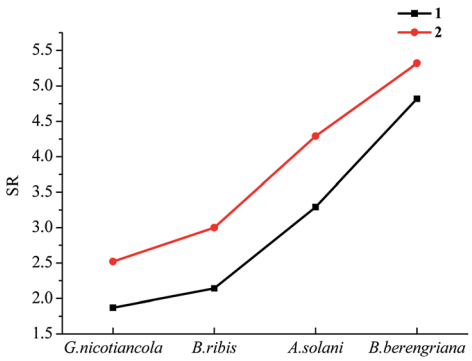

Fig. 4 Interaction (SR) between Co^{2+}, Ni^{2+} cation and tebuconazole.

leads to slightly higher bioactivities for complex **2** than complex **1** against the selected fungi. We can also obtain from Fig. 4 that both the synthesized complexes show different synergy levels to the different tested fungi. The synergy levels concerning the tested fungi is in the sequence of *B. berengriana* > *A. solani* > *B. ribis* > *G. Nicotiancola*, which implies that the antifungal activities against *B. berengriana* are improved to the greatest extent, and against *G. Nicotiancola* to the smallest extent after complexation.

2.4 Controlled release properties

The title complexes can gradually release **L** in the static water as shown in Fig. 5, suggesting that they were unstable in their coordinating mode in the aqueous solution. The releases of **L** from complexes **1** and **2** showed different rates yet similar profiles. The release rate pattern indicated that **L** from complex **1** was released more quickly than from complex **2**. For example, after 24 and 96 h in static water, complex **1** released 53.4 and 68.2% of **L**, respectively, while complex **2** released 46.9, and 57.0% of **L**, respectively.

The reason for the above difference could be related to the different stabilities of the complexes in water: the coordination bonds in complex **1** are weaker (the bond lengths of Co–N and Co–Cl in complex **1** are longer than those of Ni–N and Ni–Cl in complex **2**), which led to complex **1** being more unstable in water. The release rate of **L** from both the complexes decreased dramatically after about 20 h. This result suggests the possibility to develop the title complexes as new medicament for slower controlled release.

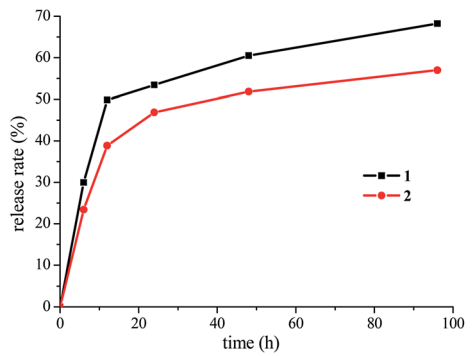

Fig. 5 Release profiles of L from complexes **1** and **2**.

2.5 DFT calculations

2.5.1 HOMO–LUMO analysis. The Frontier orbitals, highest occupied molecular orbital (HOMO) and lowest unoccupied molecular orbital (LUMO), can be used to describe electron donors and electron acceptors, which influence the bioactivity and determine the way a molecule interacts with the biological species.[33,34] The study on their Frontier orbital energy can provide useful information for the working mechanism of the bioactive compounds,[35,36] such as active sites. The Frontier orbital gap (HOMO–LUMO gap) is used as an indicator for chemical reactivity and kinetic stability of the molecule. A molecule with a small Frontier orbital gap is more polarizable and is generally associated with a high chemical reactivity and low kinetic stability.[37]

The plots of HOMO, LUMO and the energy gaps ($\Delta E = E_{LUMO} - E_{HOMO}$) of complexes **1** and **2** are shown in Fig. 6. The modes in each HOMO and LUMO are symmetrically placed as illustrated in Fig. 6. The HOMO of complex **1** is localized predominantly on Co cation, two Cl anions and two coordinated triazole rings, and the LUMO of complex **1** is localized predominantly on Co cation and two Cl anions. The HOMO and LUMO of complex **2** are very similar and localized predominantly on Ni cation, two Cl anions and four coordinated triazole rings. These results imply that the metal cations, triazole rings and coordinated Cl anions may be the reactive sites of the two complexes. The energy gaps in complex **1** and complex **2** are found to be much less (2.357 eV and 1.875 eV, respectively) than that of **L** (4.326 eV), which indicates the complexes have lower chemical activity than the ligand, and complex **2** is more reactive than complex **1**.

2.5.2 Mulliken charges analysis. It is meaningful to study the regularity of the atomic charge populations of a molecule due to its close relation to active site in its electrophilic or nucleophilic reactions and the charge interaction between two molecules.[38] The negative charges are likely to interact with the

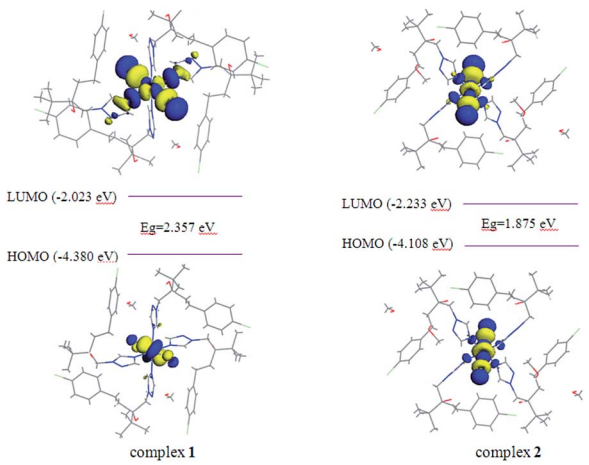

Fig. 6 HOMO and LUMO plots of complexes **1** and **2**.

positive part of the receptor. On the contrary, the positive charged parts will interact quite easily with the negatively charged part of the receptor. These interactions can play crucial role in inhibiting the growth of fungi.[39] The Mulliken atomic charges of complexes **1**, **2** and **L** obtained by means of Mulliken population analysis, are tabulated in Table 5. The center cations Co^{2+} and Ni^{2+} of the complexes gain electrons to exhibit positive charges of 0.722 e and 0.759 e, respectively. While the coordinated anions Cl^- in the two complexes lose electrons to present negative charges of −0.631 e and −0656 e, respectively. The triazole rings in the complexes with negative charges of −0.319 e, −0.336 e, respectively, also lose electrons since the triazole rings in **L** have negative charges of −0.351 e. So it can be inferred that the positive electrons transfer from the triazole rings and Cl into the metal cations. The result is responsible for the reduction of polarity of the atoms in the complexes and consequently helpful to enhance the bioactivities, because the reduction of polarity of the atoms makes contribution to the enhanced penetration of the metal complexes into the lipid membranes.[40,41]

2.5.3 Fukui function. Fukui functions are widely used local density functional descriptors to model chemical reactivity and selectivity.[42] They show the preferred regions where a chemical species will change its density when the number of electrons is modified, indicating the propensity of the electronic density to deform at a given position upon accepting of donating electrons.[43] Based on such a concept, the Fukui functions can help to identify the nucleophilic/electrophilic nature of a specific site within a molecule, which is directly related to the selectivity of the molecule towards other species.[44] Therefore, the calculations of Fukui function can also predict the active sites of the compound interacting with biological species. Fukui functions for selected atomic sites in complexes **1** and **2** have also been listed in Table 5.

Table 5 Mulliken atomic charges and Fukui functions for atoms of **1** and **2**

	Atoms	Atomic charges (e)	f_k^+	f_k^-	f_k^0
1	Co	0.722	0.263	0.134	0.199
	N1	−0.374	0.012	0.008	0.010
	C2	0.191	0.007	0.005	0.006
	N3	−0.234	0.016	0.014	0.015
	N2	−0.132	0.025	0.023	0.024
	C1	0.230	0.011	0.007	0.009
	Cl3	−0.631	0.106	0.161	0.133
2	Ni	0.759	0.187	0.093	0.140
	N1	−0.378	0.023	0.027	0.025
	C2	0.178	0.005	0.006	0.006
	N2	−0.131	0.010	0.010	0.010
	N3	−0.228	0.009	0.0100	0.009
	C1	0.223	0.008	0.008	0.008
	Cl3	−0.656	0.119	0.173	0.146
L	N1	−0.344	0.010	0.006	0.008
	C2	0.170	0.007	0.003	0.005
	N2	−0.150	0.003	0.000	0.001
	N3	−0.227	0.007	0.003	0.005
	C1	0.200	0.009	0.002	0.006

f_k^+, f_k^- and f_k^0 signs show nucleophilic, electrophilic and radical attack, respectively. The maximum values of the local electrophilic reactivity descriptors, electrophilic reactivity descriptors and radical attack reactivity descriptors at metal cations, the coordinated anions and N atoms from triazole rings of complexes **1** and **2** indicate that these sites are more reactive.

Based on the analysis above, it can be observed that the results of HOMO–LUMO, Fukui analysis and Mulliken atomic charge calculations are consistent, which indicate that the metal cations, coordinated anions and triazole rings should be the active sites of the complexes. However, previous bioactivity results show that the antifungal activities have poor correlation with the coordinated anions,[12,13] thus it may be concluded that the Co^{2+} or Ni^{2+} cations and the triazole rings originating from the ligand should be the main active sites inhibiting the growth of fungi.

2.6 Discussion of reasons for enhanced antifungal activities

As a result of the controlled release properties, the complexes release **L** step by step. The complexes can have a positive effect against the plant pathogenic fungi in a longer residual period and show different bioactivities from their ligand, which can affect the antifungal activities of the complexes. It can be further proved by the fact that complex **2** shows higher bioactivities with slower controlled release rate in comparison with complex **1**. Thereby, the controlled release properties should be one of the reasons for the enhanced bioactivities of metal complexes.

The results of DFT calculations and antifungal activities indicate that the metal cations and the triazole ring are the main active sites of the complexes against the plant fungi. While it is well known that only the triazole ring is the active site of the ligand **L**, which is also responsible for a rapid selection of resistance strains of **L**. Thus we can infer that the increased active site of the metal cations and the synergic interactions between the metal cations and **L** should be another reason for the increased bioactivities of the complexes.

Tebuconazole belongs to the ergosterol biosynthesis inhibitors, which can impair the pathogenic ability of plant fungi by destroying the structure of the cell membrane. As a result of Mulliken atomic charge calculations, the polarity of the atoms in the complexes is reduced, which is helpful for the enhanced penetration of the metal complexes into the lipid membranes and consequently enhance the bioactivities. The result is in accord with chelation theory.[10,41,42]

Therefore, the controlled release properties, the synergetic interactions between the metal cations and **L**, as well as the enhanced penetration of the metal complexes into the lipid membranes are three main reasons for the enhanced antifungal activities after complexation.

3 Experimental section

3.1 Materials and general methods

Tebuconazole was purchased from commercial source and recrystallized by isopropyl alcohol solvent. IR (KBr, σ/cm^{-1}):

3300 (m), 3140 (w), 2973 (s), 2876 (w), 1510 (vs), 1490 (vs), 1009 (s), 735 (m). All other reagents were of reagent grade and used as received. And the crystal samples of the complexes were used for all the tests. Elemental analysis was performed on a Vario EL III elemental analyzer. IR spectrum was carried out on EQUINX 55 with KBr presser bit. X-ray diffraction data were collected on a Bruker SMART APEX CCD diffractometer. Release properties were measured by high performance liquid chromatography HPLC type shimadzu LC-20A, infusion pump type LC-20ATvp, detector type SPD-20Avp, the mobile phase was methanol and water with 80% (V/V).

3.2 Procedures and synthesis of the complexes 1 and 2

3.2.1 $[CoL_4Cl_2]\cdot 4MeOH$ 1. The cobalt chloride hexahydrate (1.1897 g, 0.5 mmol) was dissolved in 5 mL methanol, and the solution was mixed with a solution of tebuconazole (0.6156 g, 2 mmol) in 10 mL methanol. The mixture was stirred at room temperature for 4 h. After 4 h, the resulting solution remained completely clear, thereafter the solution was kept at room temperature for slow evaporation. 5 days later, single crystals suitable for X-ray analysis were obtained. Yield: 71%. Elemental analysis calcd (%) for $C_{68}H_{104}Cl_6CoN_{12}O_8$ **1** (Mr = 1489.26): C 54.84, H 7.04, N 11.29; found: C 54.13, H 7.30, N l0.95. IR (KBr, σ/cm^{-1}): 3288 (m), 3134 (m), 2882 (w), 1529 (s), 1491 (vs), 1020 (m), 768 (m).

3.2.2 $[NiL_4Cl_2]\cdot 4MeOH$ 2. This complex was prepared by following essentially the same procedure for the preparation of complex **1**, except that nickel chloride hexahydrate was used instead of cobalt chloride hexahydrate. Yield: 76%. Elemental analysis calcd (%) for $C_{68}H_{104}Cl_6NiN_{12}O_8$ **2** (Mr = 1489.04): C, 54.85; H, 7.04; and N, 11.29. Found: C, 54.68 H, 7.17 and N, 11.16. IR (KBr, σ/cm^{-1}): 3291 (m), 3127 (m), 2876 (w), 1518 (s), 1492 (vs), 1015 (m), 775 (m).

3.3 Crystal structure determination

Single-crystal X-ray diffraction (XRD) measurements of **1** and **2** were carried out on a Bruker SMART APEX CCD diffractometer equipped with a graphite monochromator using Mo Kα radiation (0.71073 Å) at 296(2) K in the F–ω scan mode. Unit cell dimensions were obtained with least-squares refinements and semi-empirical absorption corrections were applied using the SADABS program.[45] The structures were solved by direct methods and refined by full-matrix least squares techniques based on F^2 with the SHELXTL program.[46] All non-hydrogen atoms were obtained from the difference Fourier map and refined with atomic anisotropic thermal parameters. The hydrogen atoms were added according to the theoretical models. Crystallographic data for structures **1** and **2** have been deposited at the Cambridge Crystallographic Data Centre as supplementary publication CCDC 934445 and 934446.†

3.4 Biological activities tests

Four important phytopathogens (*Gibberella nicotiancola*, *Botryosphaeria berengriana*, *Botryosphaeria ribis* and *Alternaria solani*) were provided by Shaanxi Microbiology Institute, China and selected for antifungal activity studies. The antifungal activities of the ligand **L**, the title complexes and the metal salts $CoCl_2\cdot 6H_2O$, $NiCl_2\cdot 6H_2O$ were diluted by starch and ground into dust, then added to potato dextrose agar (PDA) medium, respectively, to obtain a range of concentrations (1, 2, 4 and 8 mg L^{-1}) before pouring into the Petri dishes (7.5 cm in diameter).[10,47,48]

Each concentration was tested in triplicate. Parallel controls were maintained with starch mixed with PDA medium. The diameter of fungal colonies on PDA plates was measured after 72 h. Percentage inhibition of mycelial growth was calculated using the formula (1). Because the synthesized complexes can be regarded as molecular-level mixtures of **L** and inorganic salts, synergy ratios (SR) were calculated to investigate the extent of the interactions between **L** and inorganic salts according to Wadley approach[32] using the formulas (2) and (3).

$$\%\ \text{Inhibition} = \frac{\text{colony diameter of control} - \text{colony diameter of compound}}{\text{colony diameter of control}} \quad (1)$$

$$EC_{50}\ (\text{expected}) = (a + b)/(a/EC_{50}^{A} + b/EC_{50}^{B}) \quad (2)$$

$$SR = EC_{50}\ (\text{expected})/EC_{50}\ (\text{observed}) \quad (3)$$

where A, B are two antifungal components; a, b indicate the ratios of A and B to the complex, respectively: If SR ≤ 0.5, the level of interaction of single components in complex is antagonistic; if 0.5 > SR < 1.5, the level is additive; if SR ≥ 1.5, the level is synergistic.

3.5 Release assay

The release properties were carried out according to the ref. 10. Both the complexes (25 mg each sample) were placed, respectively, in 25 mL of distilled water in a beaker with film to minimize loss of water by evaporation and then allowed to stand at 28 °C. After the desired time had elapsed (6, 12, 24, 48 and 96 h), **L** released in each beaker was extracted with ether (30 mL). After ether was completely volatilized, the extract was diluted to 25 mL methanol in a 25 mL volumetric flask. The extracts were analyzed for **L** content by HPLC using calibration curves obtained from standard samples.

3.6 Computational method

The entire calculations were carried out with the DMol^3 software,[49] which is based on the density functional theory (DFT). Symmetry operations were applied for all structures. The generalized gradient approximation (GGA) of Perdew, Burke, and Ernzerhof (PBE) exchange–correlation functional[50] was used. Double numerical basis sets including polarization functions (DNP)[51,52] were performed to describe the valence orbitals of all the atoms in our calculations. To describe the cores, all-electron relativistic calculations were used.

4 Conclusion

Two new complexes of the fungicide tebuconazole, $[CoL_4Cl_2]\cdot 4MeOH$ (**1**) and $[NiL_4Cl_2]\cdot 4MeOH$ (**2**), have been synthesized

and characterized by elemental analysis, IR spectroscopy and single crystal XRD. The two complexes have similar structural geometry and both form distorted octahedron around the metal atoms. And the one-dimension chains of the complexes are formed by different kinds of hydrogen bonds. The bioactivities tests reveal that the obtained complexes are more efficient to inhibit the four selected fungi relative to the ligand tebuconazole, which indicates the potential applications of these complexes in the fields as antifungal agents. To elucidate the possible mechanism behind the increased antifungal activities, the controlled release properties and the synergistic interactions between Co^{2+}, Ni^{2+} and tebuconazole, were studied, in conjunction with theoretical investigations of the electronic structures of the complexes. The results show that the good controlled release properties, the synergic interactions between the metal cations and tebuconazole, as well as the greater penetration through the cell membrane of microorganisms all contribute to the enhanced biocidal properties. However, because of the complexity of biological systems and the limited condition of our laboratory, it is rather difficult to stipulate the detailed mechanism for the antifungal activity using the tebuconazole complexes, which may be conducted in future work.

Acknowledgements

This work is funded by the Provincial Natural Science Foundation of Shaanxi, China (Grant No. 2016JZ003). The authors would like to thank Prof. J.Z. Zhang (Department of Chemistry and Biochemistry, University of California, Santa Cruz, USA) for help in revising the manuscript.

Notes and references

1 S. S. Han, L. L. Shi, K. Li, S. Zhao, B. L. Li and B. Wu, *RSC Adv.*, 2015, **5**, 107166–107178.
2 M. H. Klingele, A. Noble, P. D. W. Boyd and S. Brooker, *Polyhedron*, 2007, **26**, 479–485.
3 X. R. Meng, Y. L. Song, H. W. Hou, H. Y. Han and B. Xiao, *Inorg. Chem.*, 2004, **43**, 3528–3536.
4 P. P. Xiong, J. Li, H. Y. Bu, Q. Wei, R. L. Zhang and S. P. Chen, *J. Solid State Chem.*, 2014, **215**, 421–435.
5 L. Habalaad, C. Bartelb, G. Giesterc, M. A. Jakupecb, B. K. Kepplerb and A. Rompela, *J. Inorg. Biochem.*, 2015, **147**, 147–152.
6 B. Q. Zou, X. Lu, Q. P. Qin, Y. X. Bai, Y. Zhang, M. Wang, Y. C. Liu, Z. F. Chen and H. Liang, *RSC Adv.*, 2017, **7**, 17923–17933.
7 N. Boechat, V. F. Ferreira, S. B. Ferreira and M. L. G. Ferreira, *J. Med. Chem.*, 2011, **54**, 5988–5999.
8 J. M. Liu, L. Wang, K. Yu, Z. H. Su, C. X. Wang, C. M. Wang and B. B. Zhou, *New J. Chem.*, 2015, **39**, 1139–1147.
9 P. D. Evans, K. J. Schmalzl, C. M. Forsyth, G. D. Fallon, S. Schmid, B. Bendixen and S. Heimdal, *J. Wood Chem. Technol.*, 2007, **27**, 243–256.
10 X. Chen and C. L. Yang, *J. Agric. Food Chem.*, 2009, **57**, 2441–2446.
11 K. Fujii, K. Hatano and Y. Kanetsuki, Preparation of difenoconazole copper salts and their use as wood preservatives, JP 2006273776A, 2006-10-12.
12 J. Li, T. Xi, B. Yan, M. Y. Yang, J. R. Song and H. X. Ma, *New J. Chem.*, 2015, **39**, 6997–7003.
13 J. Li, T. Xi, B. Yan, Y. L. Guan, M. Y. Yang, J. R. Song and H. X. Ma, *New J. Chem.*, 2015, **39**, 9550–9556.
14 Z. H. Chohan, S. H. Sumrra, M. H. Youssoufi and T. B. Hadda, *Eur. J. Med. Chem.*, 2010, **45**, 2739–2747.
15 A. K. Sadana, Y. Mirza, K. R. Aneja and O. Prakash, *Eur. J. Med. Chem.*, 2003, **38**, 533–536.
16 Y. H. Wang, D. Y. Yu, P. Xu, B. Y. Guo, Y. F. Zhang, J. Z. Li and H. L. Wang, *Ecotoxicol. Environ. Saf.*, 2014, **107**, 276–283.
17 M. Kamiya and K. Kameyama, *Chemosphere*, 2001, **45**, 231–235.
18 E. Morillo, T. Undabeytia, C. Maqueda and A. Rams, *Chemosphere*, 2002, **47**, 747–752.
19 P. Z. Zhang, Q. Y. Fu, R. X. Chi, C. X. Yang and J. G. Xu, *J. Zhejiang Univ. Sci. Technol.*, 2003, **15**, 142–145, (in Chinese).
20 Z. Kang, L. Huang, U. Krieg, A. Maulermachnik and H. Buchenauer, *Pest Manage. Sci.*, 2001, **57**, 491–500.
21 J. P. Zubrod, M. Bundschuh, A. Feckler, D. Englert and R. Schulz, *Environ. Toxicol. Chem.*, 2011, **30**, 2718–2724.
22 C. Wang, F. Wang, Q. Zhang and W. Liang, *Eur. J. Soil Biol.*, 2016, **72**, 6–13.
23 R. Akallal, D. Debieu, C. Lanen, M. J. Daboussi, R. Fritz, C. Malosse, J. Bach and P. Leroux, *Pestic. Biochem. Physiol.*, 1998, **60**, 147–166.
24 R. D. Horsley, J. D. Pederson, P. B. Schwarz, K. McKay, M. R. Hochhalter and M. P. McMullen, *Agron. J.*, 2006, **98**, 194–197.
25 L. Lucini and G. P. Molinari, *Pest Manage. Sci.*, 2009, **65**, 440–443.
26 I. D. Brown and D. Altermatt, *Acta Crystallogr., Sect. B: Struct. Sci.*, 1985, **41**, 244–247.
27 S. Gao, X. F. Zhang, L. H. Huo, Z. Z. Lu, H. Zhao and J. G. Zhao, *Acta Crystallogr., Sect. E: Struct. Rep. Online*, 2004, **60**, 1128–1130.
28 J. Matsumoto, T. Suzuki, Y. Kajita and H. Masuda, *Dalton Trans.*, 2012, **41**, 4107–4117.
29 F. D. Salvo, F. Teixidor, C. Viñas, J. G. Planas, M. E. Light, M. B. Hursthouse and N. Aliaga-Alcalde, *Cryst. Growth Des.*, 2012, **12**, 5720–5736.
30 Y. Q. Huang, B. Ding, H. L. Gao, P. Cheng, D. Z. Liao, S. P. Yan and Z. H. Jiang, *J. Mol. Struct.*, 2005, **743**, 201–207.
31 S. L. Gao, Q. Yang, J. L. Li, G. Fan, X. X. Li, L. P. Chen, X. T. Dang and Z. Y. Wu, *Periodic Table of Chemical Element*, Science Press, Beijing, 3rd edn, 2012, (in Chinese).
32 F. M. Wadley, *Experimental Statistics in Entomology*, Graduate School Press, Washington State University, Pullman, 1976.
33 J. X. Mu, Z. W. Zhai, M. Y. Yang, Z. H. Sun, H. K. Wu and X. H. Liu, *Crystals*, 2016, **6**, 4.
34 M. Larif, A. Adad, R. Hmammouchi, A. I. Taghki, A. Soulaymani, A. Eimidaoui, M. Bouachrine and T. Lakhlifi, *Arabian J. Chem.*, 2017, **10**, S946–S955.
35 J. X. Mu, Y. X. Shi, M. Y. Yan, Z. H. Sun and X. H. Liu, *Molecules*, 2016, **21**, 68.

36 W. Boufas, N. Dupont, M. Berredjem, K. Berrezag, I. Becheker, H. Berredjem and N. E. Aouf, *J. Mol. Struct.*, 2014, **1074**, 180–185.
37 J. Aihara, *J. Phys. Chem. A*, 1999, **103**, 7487–7495.
38 P. Govindasamy, S. Gunasekaran and S. Srinivasan, *Spectrochim. Acta, Part A*, 2014, **130**, 329–336.
39 K. C. Zheng, J. P. Wang, W. L. Peng, Y. Shen and F. C. Yun, *Inorg. Chim. Acta*, 2002, **328**, 247–253.
40 A. Chaudhary, N. Bansal, A. Gajraj and R. V. Singh, *J. Inorg. Biochem.*, 2003, **96**, 393–400.
41 C. R. A. María, C. L. S. Estefania, S. Jesús, P. Pelagatti and F. Zani, *J. Inorg. Biochem.*, 2005, **99**, 2231–2239.
42 K. Fukui, T. Yonezzawa and H. Shingui, *J. Chem. Phys.*, 1952, **20**, 722–725.
43 C. J. Brala, I. Fabijanić, A. K. Marković and V. Pilepić, *Comput. Theor. Chem.*, 2014, **1049**, 1–6.
44 S. Saravanan and V. Balachandran, *Spectrochim. Acta, Part A*, 2014, **130**, 604–620.
45 G. M. Sheldrick, *SADABS*, University of Göttingen, Germany, 2000.
46 G. M. Sheldrick, *Acta Crystallogr., Sect. A: Found. Crystallogr.*, 2008, **64**, 112–122.
47 D. Saetae and W. Suntornsuk, *J. Microbiol. Biotechnol.*, 2010, **20**, 319–324.
48 R. K. Devappaa, S. K. Rajeshb and V. Kumara, *Ecotoxicol. Environ. Saf.*, 2012, **78**, 57–62.
49 B. Delley, *Phys. Rev. B: Condens. Matter Mater. Phys.*, 2002, **65**, 85403–85409.
50 J. P. Perdew, K. Burke and M. Ernzerhof, *Phys. Rev. Lett.*, 1996, **77**, 3865.
51 B. Delley, *J. Phys. Chem.*, 1996, **100**, 6107–6110.
52 W. J. Hehre, L. Radom, P. V. R. Schlyer and J. A. Pople, *Ab Initio Molecular Orbital Theory*, Wiley, New York, 1986.